Role of Electrical Double Layer Structure in Ionic Liquid Gated Devices

Jennifer M. Black,[†,∇] Jeremy Come,[†,○] Sheng Bi,[‖] Mengyang Zhu,[‖] Wei Zhao,[‖] Anthony T. Wong,[⊥] Joo Hyon Noh,[⊥] Pushpa R. Pudasaini,[⊥] Pengfei Zhang,[‡] Mahmut Baris Okatan,[†] Sheng Dai,[‡,#] Sergei V. Kalinin,[†] Philip D. Rack,[†,⊥] Thomas Zac Ward,[§] Guang Feng,[*,‖] and Nina Balke[*,†]

[†]Center for Nanophase Materials Sciences, [‡]Chemical Sciences Division, and [§]Materials Science and Technology Division, Oak Ridge National Laboratory, Oak Ridge, Tennessee 37831, United States

[‖]State Key Laboratory of Coal Combustion, School of Energy and Power Engineering, Huazhong University of Science and Technology (HUST), Wuhan 430074, China

[⊥]Department of Materials Science and Engineering and [#]Department of Chemistry, University of Tennessee, Knoxville, Tennessee 37996, United States

S Supporting Information

ABSTRACT: Ionic liquid gating of transition metal oxides has enabled new states (magnetic, electronic, metal−insulator), providing fundamental insights into the physics of strongly correlated oxides. However, despite much research activity, little is known about the correlation of the structure of the liquids in contact with the transition metal oxide surface, its evolution with the applied electric potential, and its correlation with the measured electronic properties of the oxide. Here, we investigate the structure of an ionic liquid at a semiconducting oxide interface during the operation of a thin film transistor where the electrical double layer gates the device using experiment and theory. We show that the transition between the ON and OFF states of the amorphous indium gallium zinc oxide transistor is accompanied by a densification and preferential spatial orientation of counterions at the oxide channel surface. This process occurs in three distinct steps, corresponding to ion orientations, and consequently, regimes of different electrical conductivity. The reason for this can be found in the surface charge densities on the oxide surface when different ion arrangements are present. Overall, the field-effect gating process is elucidated in terms of the interfacial ionic liquid structure, and this provides unprecedented insight into the working of a liquid gated transistor linking the nanoscopic structure to the functional properties. This knowledge will enable both new ionic liquid design as well as advanced device concepts.

KEYWORDS: transistor, liquid gating, scanning probe microscopy, ionic liquid, electric double layer
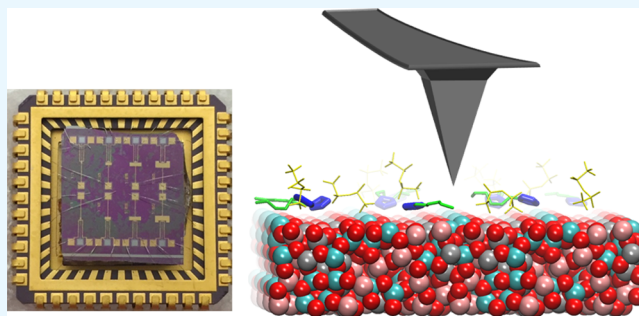
INTRODUCTION

Understanding the fundamental physics of functional oxides brings forth the challenge of separating the chemical, electronic, and lattice degrees of freedom, fully coupled in bulk materials. Under an external stimulus, collective state switching and new electronic phases can result in new ways to write, store, and process information. In particular, transition metal oxides possessing a partially filled d-electron band have been studied for memory or neuromorphic devices, because of their ability to exhibit fast and abrupt electronic and/or structural transitions.[1,2] For metal−insulator transitions, the electronic state is governed by the competition between electron localization and delocalization, which can be controlled by stress, thermal energy, optical excitation, or electric field.[3,4] For most materials reported, their complex phase diagrams cannot be explained by one single driving force but rather by the cooperation of multiple interactions.[5−7] Along with the efforts for designing

materials capable of switching in ambient conditions with minimal energy requirement, the development of field-effect transistors (FETs) allowed the opportunity to create new states of matter controlled by high electric field gating phenomena.[8,9] Electric double layer (EDL) transistors using ionic liquids (ILs) or ion gels as dielectric media have gained attention by inducing and maintaining charge accumulation as high as 8.0×10^{14} cm^{-2} at the solid−liquid interface, competing with that achieved with high k solid state dielectrics.[10−16] The charge accumulation occurs by applying an electric field across the IL, together with the formation of an EDL, which changes the properties of the underlying gating material. Other electro-chemically-controlled diodes work on the principle of
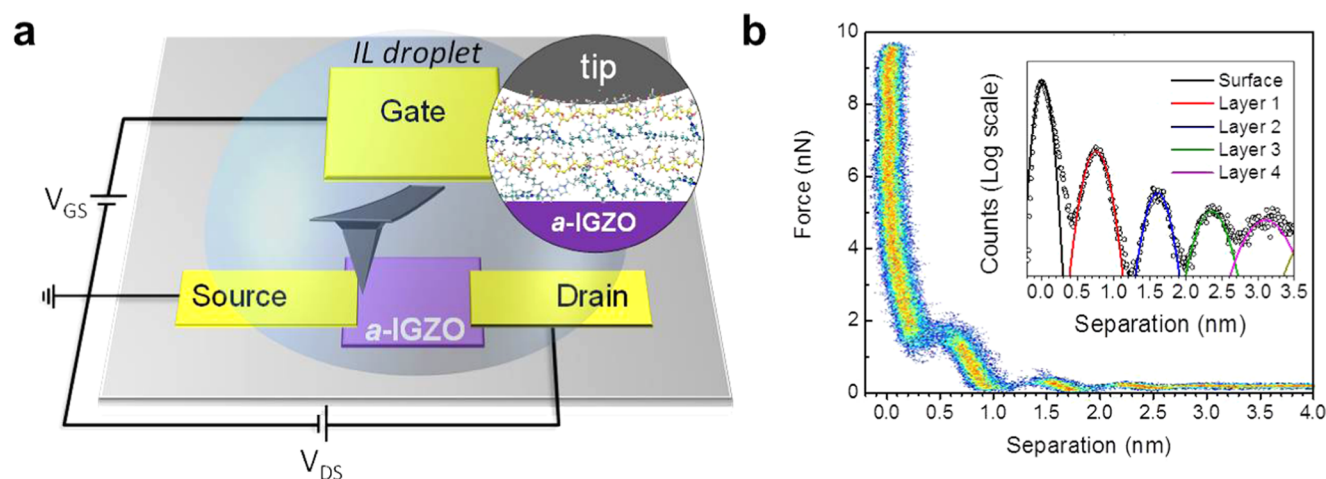
Figure 1. IL-gated a-IGZO FET. (a) Schematic illustration of the device with the AFM tip located close to the source electrode. (b) Two-dimensional (2D) histogram of 50 force−distance approach curves at zero gate and drain voltage. Inset shows the corresponding separation histogram used in this study, with ion layer peaks fitted with Gaussian function.

electronic current gating through single molecules forming nanojunctions.[17−21]

Recently, IL-gated amorphous metal oxide films showed excellent transistor performance, with field-effect carrier mobilities in excess of 20 cm^2/V/s, and threshold voltages and subthreshold swing as small as 0.5 V and 0.1 V/decade, respectively, which compare favorably to those of conventional solid state oxide-gated FETs.[22,23] In these devices, the EDL can be used as a physical tool for tuning the electronic states of inorganic metal oxide semiconductors,[24] therefore its structure is an important issue because the screening of the excess surface charge is governed by the arrangement and conformation of ions. To date, however, the distinct electronic states of the underlying material have not been correlated with the changes in the EDL structure of the interfacial IL. The amorphous indium gallium zinc oxide thin film transistor is an n-channel device where accumulation of charge carriers occurs in the oxide upon application of a positive gate voltage,[25] and it forms an ideal platform to characterize and correlate the device characteristics and the IL structure because its turn-on characteristics have been well-characterized.[26,27] Understanding the interplay between the EDL structure and the transistor behavior of the oxide channel is thus crucial for our comprehension of the charge carrier enhancement at the interface and how it affects the conductivity of the oxide film.

EDL structure and dynamics of ILs at neutral and electrified surfaces have been extensively studied experimentally[28−34] and computationally.[35] The electrostatic interactions and van der Waals forces induce ion ordering at the solid−IL interface, leading to the formation of alternating layers of cations and anions on the surface. This lamellar arrangement in the EDL extends in successive layers to several nanometers in the solution, and it is governed by a steric effect from the finite size of the ions and a Coulombic effect from their charge.[36] When an electric potential is applied to the electrode, the interfacial layer changes from cation-rich to anion-rich when the surface potential switches from negative to positive, respectively.[37,38] Basically, two processes have been described: (i) overscreening of ions when the charge of the first layer is larger than that of the electrode potential, and (ii) crowding of counterions at the surface when the charge of the innermost layer is lower than that of the surface potential.[39,40] In addition to the

accumulation of counterions in the innermost layer, integrated experimental and computational studies suggested that the charge screening in the liquid phase occurs via preferential orientation of ions that minimize the EDL thickness.[41−43] Surprisingly, the literature reporting ion layering at metal oxide surfaces is scarce,[44] and furthermore, no experimental studies of the IL structure at metal oxide surfaces have been published. On electrified surfaces, the bias-dependent ion arrangement in the EDL is a consequence of the applied voltage and corresponding surface charge. On nonmetallic surfaces, the situation is reversed, and the structure of the EDL can alter the properties of the surface. In such situations, the structure of the EDL and thus the functional material properties can be changed through electric fields applied to additional electrodes, as is done in FETs. However, the interplay between EDL structure and the surface properties of nonmetallic surfaces has not been studied. Therefore, the EDL structure and its impact on the gating process in liquid FETs remain unknown, although this understanding is crucial to understanding and improving the mechanisms underpinning operation of those devices.

Here, we study the structure of a 1-hexyl-3-methylimidazolium bis(trifluoromethylsulfonyl)imide (HMImTFSI) ionic liquid used to gate an amorphous indium gallium zinc oxide (a-IGZO) semiconducting channel by atomic force microscopy (AFM) coupled with atomistic molecular dynamics (MD) simulations. For this study, a nonspherical cation with π−π stacking was chosen, because nonspherical molecules are the most widely used in ionic liquid gating work and are the best characterized ionic liquids.[45] As opposed to spherical molecules, orientation changes can be readily observed through changes in distance between the electrode surface and the absorbed ion layers.[42] Using force spectroscopy techniques, the out-of-plane ordering (perpendicular to the oxide surface) of ionic layering was measured at various gate-source voltages, and correlated with both applied electric field and the semiconducting oxide electrical properties. The measured ion positions and their correlation to differently oriented ions in the EDL are further revealed by MD modeling.

■ RESULTS AND DISCUSSION

The position of ion layers was measured via an AFM technique using static force−distance curves on the device itself inside an
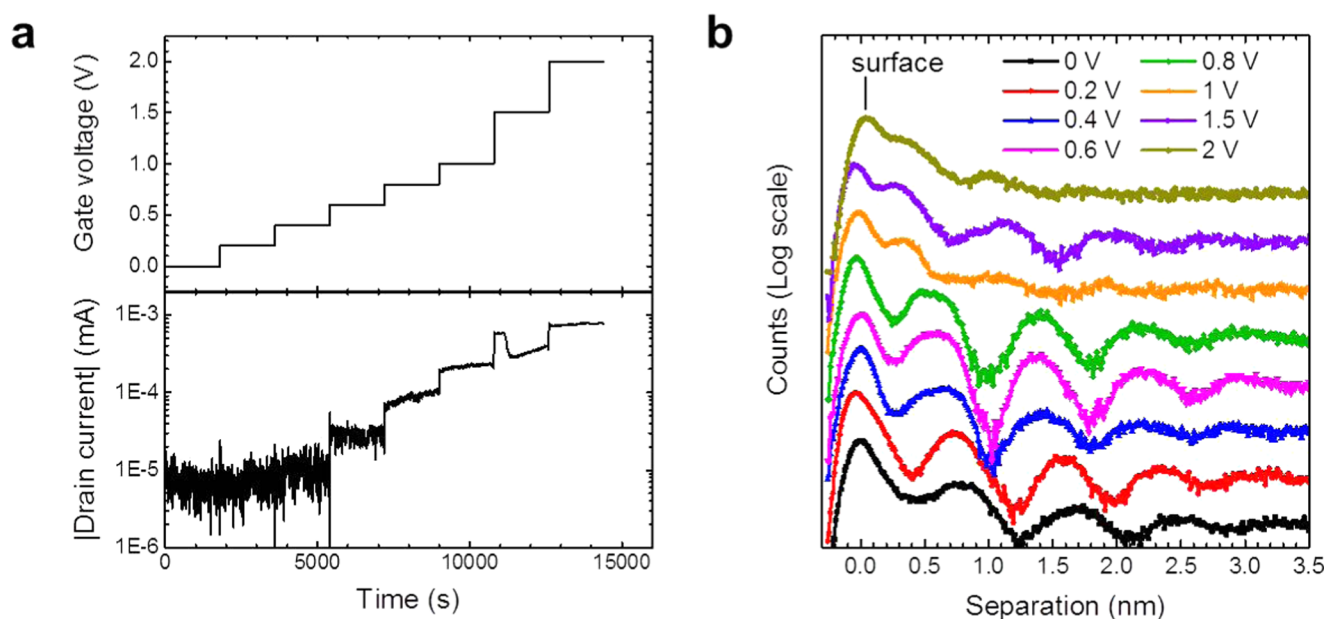
Figure 2. Gate voltage dependence of ionic layering at a-IGZO surface. (a) Applied gate voltage and measured drain current as a function of time (0.1 V drain bias). (b) Separation histograms at different gate voltages.
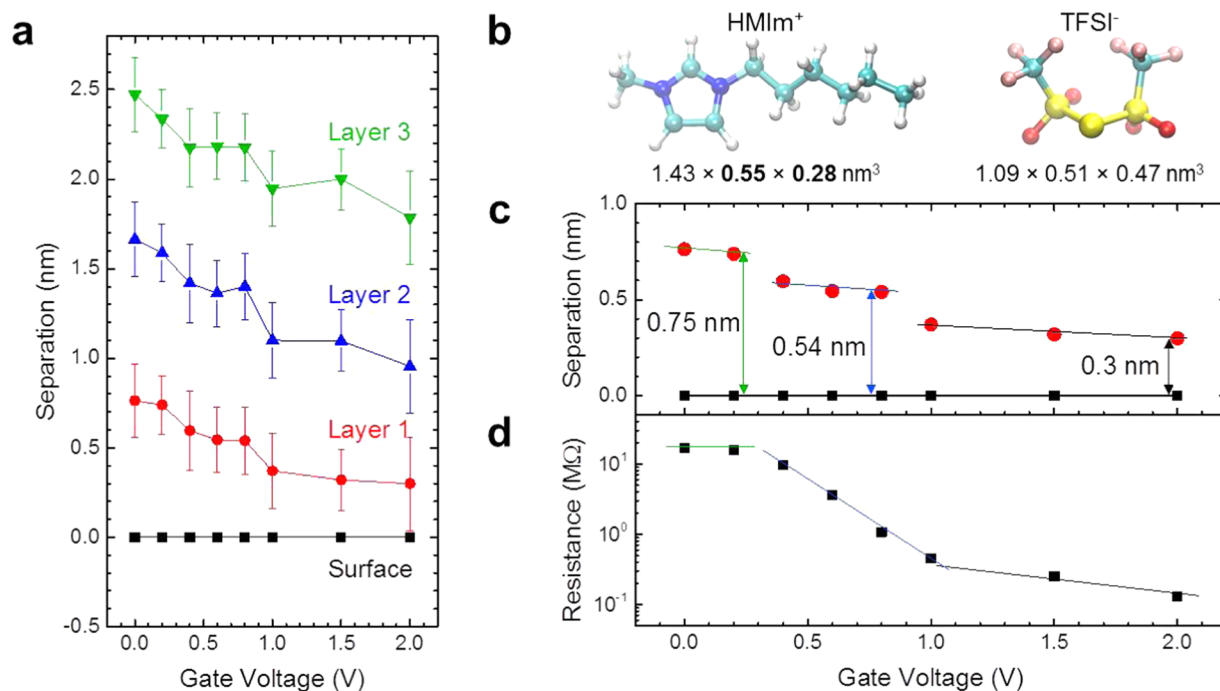

Figure 3. Separation distances of the different ion layers as a function of gate voltage. (a) Separation distances of the first three ion layers as a function of gate voltage with a constant 0.1 V drain bias. The error bars reflect the full width at half maximum of each histogram peak. (b) Schematic illustrations of HMIm$^+$ and TFSI$^-$ geometries with lateral dimensions. (c) Separation distance of the first ion layer and (d) calculated resistance of the oxide channel as a function of gate voltage, respectively.

ionic liquid droplet close to the source gold electrode (Figure 1a). During the approach, discontinuities in the force−distance curves can be clearly identified before the tip reaches the sample surface, where no further discontinuities can be observed. To investigate the quantitative significance of the spacing, we used separation histograms of 50 consecutively measured force−distance curves (Figure 1b). The observed force oscillations are formed by the repulsive interaction forces between the AFM tip and the ion layers while the cantilever is approaching the oxide surface. For further analysis, only the separation values are considered and plotted on a log scale clearly illustrating the separation peaks (inset in Figure 1b). Each peak representing an ion layer was then fitted with a Gaussian function to extract the corresponding layer position from the maximum. The experimental data enables identification of at least four distinct ion layers at ca. 0.8, 1.6, 2.4, and 3.2 nm from the surface at zero gate voltage. These distances cannot clearly be assigned to the dimensions of one anion−cation unit, or to a single ion monolayer with dimensions of $1.43 \times 0.55 \times 0.28$ nm^3 and $1.09 \times 0.51 \times 0.47$ nm^3 for
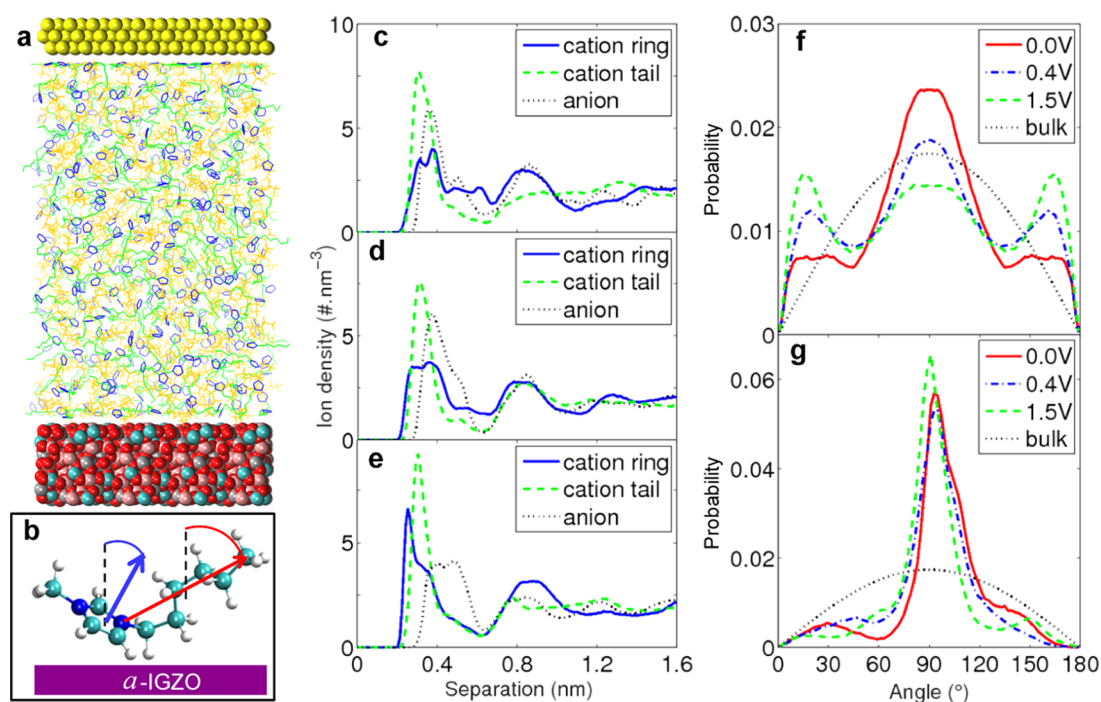
Figure 4. Molecular dynamics simulation of HMImTFSI structure at a-IGZO surface. (a) Snapshot of simulation system, in which the HMIm$^+$ cation is shown with a blue ring and green tail and the TFSI$^-$ anion is represented by orange lines. (b) Schematics of imidazolium ring and alkyl tail spatial and angular positions with respect to the a-IGZO surface. Cation ring, tail, and anion density profiles, based on the center of the ring and tail respectively, at (c) 0 V, (d) 0.4 V, and (e) 1.5 V. Angular distributions of the (f) imidazolium ring and (g) alkyl tail in the first cation layer.

HMIm$^+$ and TFSI$^-$, respectively.[46] To identify the nature of the measured ion position, comparison with MD for highly oriented pyrolytic graphite surfaces and Mica showed that the measured ion position matches with the cation or anion layer depending on the geometric volume of the ion.[47] However, comparable studies on ILs at the metal oxide surface do not currently exist, either in experiment or by simulation. It was proposed that the EDL structure of ILs with long alkyl chains (and thus more amphiphilic) consists of bilayers of cations, due to the aggregation of the nonpolar groups with neutralizing layers of anions adjacent to the imidazolium groups.[48] Nevertheless, the presence of the oscillatory forces attests to a repeating ordered structure in the IL, and its evolution will be studied hereafter. In the present case, the force required to pass through one layer is spread across a broad separation distance, as opposed to previously reported studies, where sharp transitions were measured.[49] This may originate from molecular arrangements taking place to accommodate the strain in the confined space between the tip and the surface. Indeed, the ions used in this study are highly asymmetric, and therefore prone to minimize their conformational occupancy by optimizing their spatial orientation. Particularly, the long neutral alkyl chain of the HMIm$^+$ cation creates voids that can be replaced by charged groups via rotation and translations of ions.[50] The energy barrier between the layers decreases further away from the surface, indicating that the lamellar structure becomes more disordered toward the bulk liquid.

The possibility to detect ion layers in the EDL of the ionic liquid on the oxide surface can be used to explore the changes in its structure induced by varying the gate voltage. Figure 2a shows that the drain−source current for each gate voltage step increases from ∼5 nA to ∼1 μA, which is consistent with the values previously reported.[22,51] When the gate voltage is

increased, all ion layers progressively shift toward the oxide surface, as displayed in Figure 2b.

The measured ion layer positions with respect to the surface were fitted as Gaussian peaks (as demonstrated in Figure 1b), and analyzed as a function of gate voltage. Interestingly, change in ion layer position does not simply follow a continuous reorganization, but rather undergoes abrupt transitions at ∼0.4 and ∼1 V (Figure 3a). For the innermost ion layer (Figure 3c), the separation of 0.75 nm at 0 V decreases to 0.59 nm at 0.4 V. Another abrupt displacement closer to the surface is observed at 1 V, with separation distance sharply decreasing to 0.37 nm. Between these steps, only gradual displacements toward the oxide surface are measured, attesting to minimal ordering occurring at higher gate voltage.

On the basis of the measured dimensions of the innermost ion layer, the transitions can be explained in terms of different orientations of the HMIm$^+$ cation at the surface, together with expulsion of the remaining TFSI$^-$ coions. Indeed, both 0.54 and 0.3 nm separation distances are close to two transverse dimensions of the HMIm$^+$ ion (Figure 3b), whereas none of the TFSI$^-$ anion lengths seem to correspond; this suggests that the cation orientations at the a-IGZO surface are strongly dependent on the positive polarity electric field, and can be controlled with the gate voltage. To highlight the correlation of the interfacial liquid structure with the gating properties, the resistance of the a-IGZO channel was calculated from the applied source−drain voltage and measured source−drain current at each gate voltage measured (Figure 3d). The sigmoidal shape transition between states of different conductivity is consistent with the three distinct stages of the separation distances of the innermost IL layer. In a previous publication on the same sample system, it was shown that the carrier mobility does change with gate voltage.[51] The curve for mobility as a function of gate voltage showed different slopes in
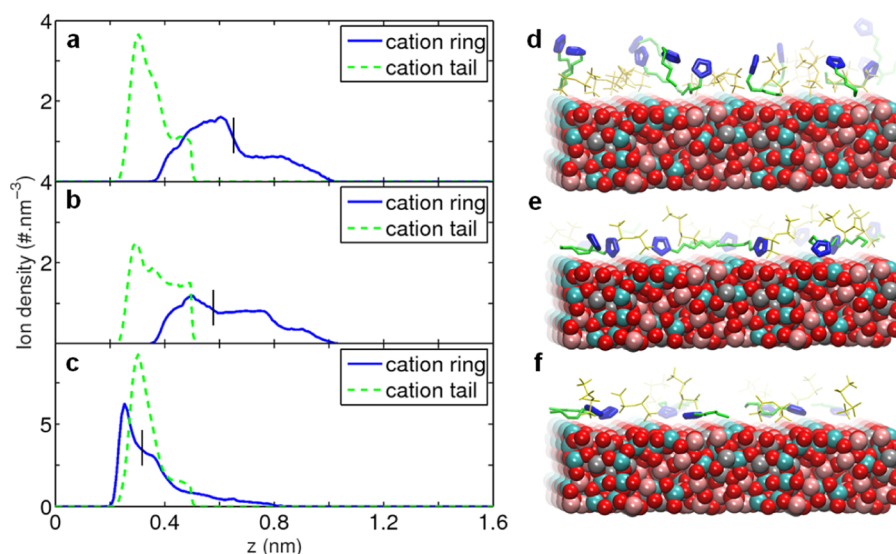
Figure 5. Structure of the first adsorbed HMim$^+$ layer on the a-IGZO surface as function of voltage. HMim$^+$ cation tail and ring density profiles at (a) 0 V, (b) 0.4 V, and (c) 1.5 V. Snapshots of the corresponding innermost ion layer structure at (d) 0 V, (e) 0.4 V, and (f) 1.5 V.

different voltage regimes that are overlapping with the regimes observed for the ion reorientation. This demonstrates a clear connection between the structure of the EDL and the device properties, thus linking nanoscale and macroscale phenomena that have not been demonstrated previously. However, the exact correlations between field-dependent IL capacitance and the carrier mobility in a-IGZO requires more detailed measurements, which will be the subject of future studies.

To understand the experimental findings and test the aforementioned hypothesis, molecular dynamics (MD) simulations were performed to investigate the HMImTFSI structure at the a-IGZO surface and its evolution under varying gate voltage. For a reliable comparison between modeling and experiments, we built up an MD simulation system based on an IL channel enclosed between Au(111) and a-IGZO walls (Figure 4a). The amorphous phase of the IGZO material was obtained by quenched molecular dynamics (QMD) simulation from the crystalline phase (see SI-1 in Supporting Information and Methods section for more details on the generation of the amorphous IGZO and MD simulations), and constant voltages (0, 0.4, and 1.5 V) were applied on both walls contacting the IL. Note that the potential applied between the gold and a-IGZO surfaces acts across the IL slab and does not include the potential drop across a-IGZO. When the gate voltage V_{GS} is small and a-IGZO is highly resistive, the potential drop across the IL slab V_{IL} is nearly zero. When V_{GS} is large and the oxide is in a highly conductive state ($V_{GS} > 1.0$ V in this work), V_{IL} is almost equal to V_{GS}. In the case of intermediate V_{GS}, there is a certain potential drop across a-IGZO and $V_{IL} < V_{GS}$. Specifically, the potential across the IL slab used in simulations of 0, 0.4, and 1.5 V corresponds to gate voltages of 0, 0.7, and 1.5 V, respectively (see Supporting Information for more details).

Because of the high asymmetry of the HMim$^+$ molecule, we analyzed the number density and spatial orientations of both imidazolium ring and alkyl chain positions separately, as depicted in Figure 4b. The ion density profiles in Figure 4c−e show the alternating cation−anion layering of the interfacial IL, which is consistent with the structure revealed experimentally for ILs at oxides.[33,34] With increasing applied voltage, HMim$^+$ cations accumulate in and TFSI$^-$ anions are squeezed out from

the innermost layer, indicating an increase in cation density with increasing voltage. Such packing of interfacial cations occurs together with important changes in the molecular orientations (Figure 4f,g), suggesting that (i) at 0 V, the cations tend to be either vertical or parallel to the surface, contrasting with most cations being flat on the Au(111) surface (Figure S3), and (ii) with increasing gate voltage, the imidazolium rings adopt a configuration parallel to the surface, thus decreasing the separation distance. Interestingly, the total number of adsorbed cations in the simulation box varies little (30.3, 31.5, and 31.5 at 0, 0.4, and 1.5 V, respectively), indicating that (i) the charge compensation in the double layer is dominated by anion removal, and (ii) the ion orientation rather than the ion number is of importance for changes in charge density on the oxide surface.

A significant fraction of HMIm$^+$ cations already lay flat at the surface when no voltage is applied (Figures 4f,g and S4), and thus, they do not contribute to the changes in the force−separation curves. In Figure 5, the adsorbed layer was isolated by removing the horizontal cations (tail and ring parallel to the surface, see details in SI-3, Figure S5) for a more detailed examination of its bias dependence. This enables a better comparison with the experimental results because the force signal likely derives from the nonhorizontally aligned cations (the approaching AFM tip is more sensitive to the imidazolium rings than the flexible alkyl tail). As a result, the average ring center position is located at 0.63 ± 0.06 nm at 0 V (Figure 5a), and decreases to 0.58 ± 0.05 nm at 0.4 V (Figure 5b). When further increasing the gate voltage to 1.5 V (Figure 5c), most cations are flat on the surface, with the average center position at ∼0.31 ± 0.02 nm. These simulation results strongly support the mechanism suggested by the AFM experiments in which the measured separation distances match specific cation orientations that compensate for the increasing field strength. Indeed, the corresponding interfacial ionic structure at 0 V (Figure 5d) shows that the cations are arranged in a random fashion and the surface−ion spacing does not match a specific ion dimension, but rather the average of the three. Upon increasing the gate voltage, the displacement of cations closer to the surface takes place in two steps: (i) more alkyl chains rotate horizontally due to the attraction of the rings to the
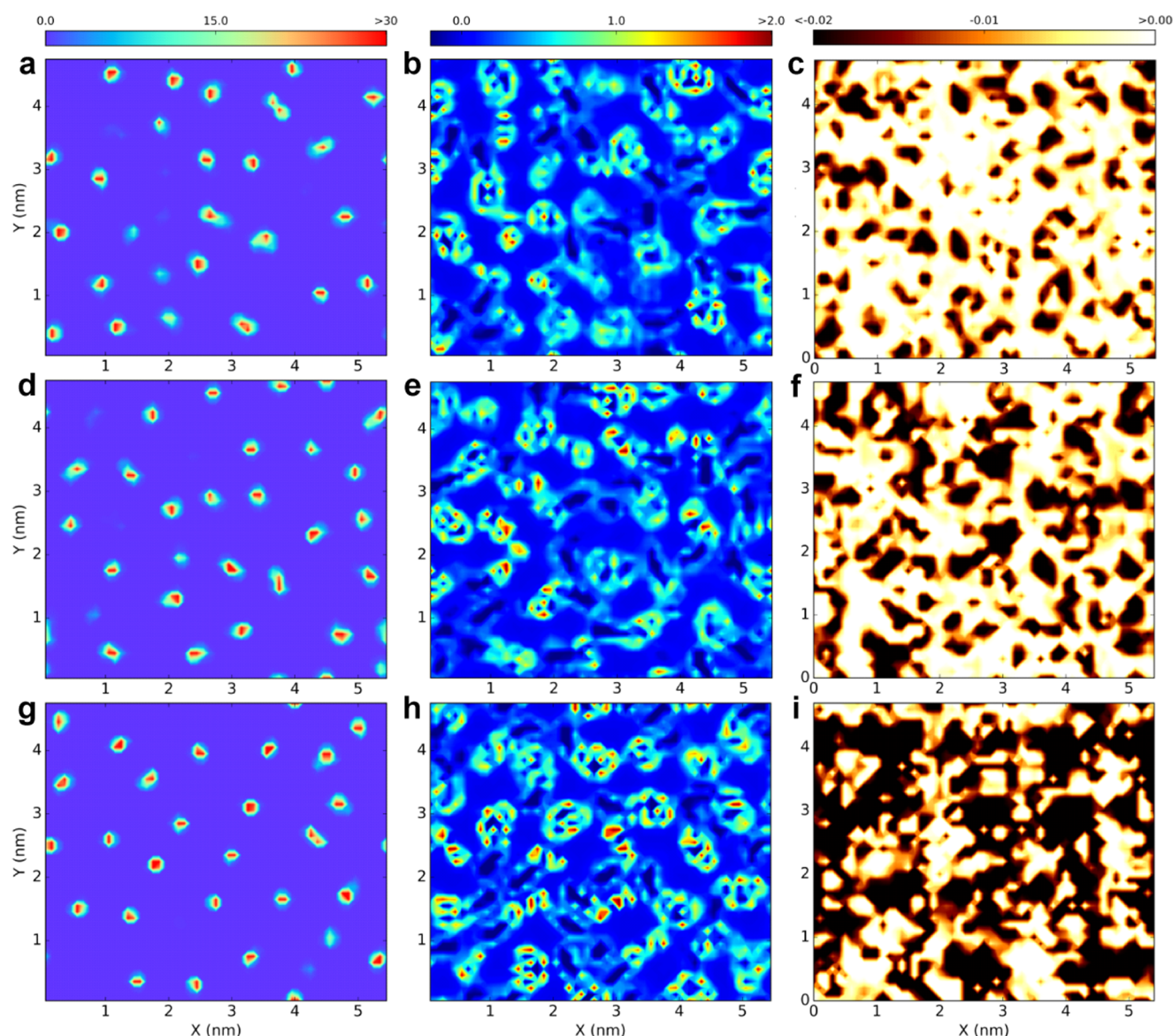
Figure 6. Influence of interfacial counterions on charge distribution at a-IGZO surface with voltage variation. Left column (a, d, g): 2D number density of cations in the first layer (unit: #/nm^2); middle column (b, e, h): 2D charge density of cations in the first layer (unit: C/m^2); right column (c, f, i): charge distribution on the a-IGZO surface (unit: C/m^2) across the entire EDL. Top row (a−c): 0 V; middle row (d−f): 0.4 V; bottom row (g−i): 1.5 V.

charged a-IGZO (Figure 5e), and (ii) the imidazolium rings tilt parallel to the surface, minimizing the measured separation distance (Figure 5f). Thus, the change in the ionic arrangement via cation flattening at high gate voltage results in a decrease of the EDL thickness. Similar observations have been reported for highly oriented pyrolytic graphite surfaces, where dense and flat-oriented counter-ion layers form upon bias.[42]

To understand the IL-gate-induced conductance of a semiconductor, based on experimental observations of IL-gated SrTiO$_3$ (STO), Parkin and co-workers proposed that imperfectly distributed cations create inhomogeneous charge carries to form disconnected metallic regions on the STO surface under low gate voltage. With increasing gate voltage, such metallic regions would become connected, resulting in the metallic behavior of the device.[52] With the help of MD simulation, we investigated surface-adsorbed cations and the generated surface charge of the a-IGZO surface by analyzing the 2D density and charge distribution within the first counter-

ion layer parallel to the oxide surface at different gate voltages. Counterions (cations here) were found to distribute in an indistinct pattern at the a-IGZO surface, when the potential across the IL slab is 0 V, as shown in Figure 6a. The charges from the counterions distribute in a less-defined pattern at the a-IGZO surface, as shown in Figure 6b. Note that these charges are only the charges of the first ion layer and not the entire double layer. This is because ionic liquids are quite different from a conventional electrolyte (e.g., NaCl aqueous solution), which has small and "roundish" ions with uniform charge distribution (i.e., the ion has all of the charge on one atom), and IL ions usually have large sizes with asymmetric shapes, and their molecular charge density is highly irregular and delocalized among their atoms. Conceptually, the EDL consists of the layer of surface charges and counterions.[53] Hence, we further investigated the charges accumulating at the a-IGZO surface from simulation analysis, as shown in Figure 6c. This includes all charges in the EDL across multiple ion layers. It was

found that the charge distribution increases with increasing gate voltage and is not homogeneous, i.e., the electrons concentrate in some regions of the a-IGZO surface to form disconnected metallic regions instead of being distributed across the whole surface uniformly. Although the charge distribution at the a-IGZO surface is strongly correlated with the local charge distribution of counterions in the first layer, this inhomogeneity has a different pattern from Figure 6b. This is because of the fact that the charge on the a-IGZO surface not only correlates with charges from cations but is also influenced by other ions beyond the first cation layer, because the IL-based EDL has a complex structure with more than one ion layer. As the potential across the IL slab increases to 0.4 V (which corresponds to V_{GS} = 0.7 V), the cation number density changes slightly (Figure 6d) and the charge density in the cation layer changes somewhat (Figure 6e). However, the charge distribution at the a-IGZO surface changes significant, i.e., more metallic regions with larger size (Figure 6f). A similar scenario but with more distinct contrast was found when the potential across the IL slab reached 1.5 V (Figure 6g−i). Interestingly, the metallic regions become connected to form percolation paths, resulting in the metallic behavior of the device. This inhomogeneity from either IL side (cations and their charge distributions) or a-IGZO side (surface charge distribution), as revealed by MD simulation, is the first time the behavior observed by Parkin and co-workers[52] could be explained. Because Parkin et al. worked with single-crystalline materials, additional mechanisms could be used to explain their observation of inhomogeneous charge distribution that are independent of the results shown here. However, simulations on graphite have confirmed the presence of charge fluctuations even in highly ordered systems.[54] Moreover, the number density changes only slightly with voltage varying from 0 to 1.5 V (Figure 6a,d,g). This seems to stand in contrast to Figure 4c−e, which shows an increase in cation density with increasing voltage. Figure 4 displays the one-dimensional ion density normal to the surface and separates the different parts of the cation, whereas Figure 6a,d,g shows the 2D ion density parallel to the surface, which was analyzed based on the center of the molecule where the atomic information could not be fully reflected. In contrast, the 2D charge densities (Figure 6b,e,h) were calculated from each atom, thus the charge distributions are more detailed and have distinct differences with voltage variation. The full picture of the change in ion density with increasing voltage is a combination of the information available in both Figures 4 and 6.

The present work undoubtedly evidences the intricate interplay between the interfacial ionic structure and consequent field-effect transistor behavior. Under the influence of the applied gate voltage, the highly packed cation layer at the surface generates large local charge densities, leading to significant enhancement in the oxide conductivity. This can be explained by MD simulation demonstrating the reorientation of cations and the resulting local charges on the IGZO surface. The reorientation of charges matches the experimental observation obtained with atomic force microscopy force−distance curves. In the future, a more detailed picture of the ion layers throughout the entire oxide channel needs to be established, and this will be the focus of future studies utilizing the x-y scanner in AFM to access different channel locations. Further modeling efforts will study the effect of different charge densities inside the EDL on the electronic structure of the oxide material for all gate voltages, especially the intermediate voltage

ranges. In general, measuring the ion layering and the correlation with macroscopic device performance opens up the pathway for improving the device performance by advanced ionic liquid design. This can include cation and anion dimension as well as charge distribution across the ions. The presence of interfacial layers or oxides with different termination could also be used to actively influence the ion orientation in the EDL. Through this, new physics and enhanced device properties can be explored and realized.

■ CONCLUSIONS

In summary, we have successfully demonstrated that the interface of the HMImTFSI ionic liquid undergoes strong and orderly rearrangement during the gating process of a semiconducting a-IGZO channel. The force spectroscopy experiments together with molecular dynamics simulations clearly evidence that the preferential arrangement of the innermost cations correlate to the different electronic states of the oxide material. This strongly suggests that the conductivity of the film is governed by the shrinking of the EDL thickness via cation reorientation and anion expulsion. These results are important because they show great promise toward better control of the switching properties via the proper design of the solid/ionic liquid interface.

■ METHODS

Device Preparation. The a-IGZO FET devices were fabricated by standard photolithographic patterning processes. First, a chromium (Cr) back gate metal (150 nm) was sputter deposited on a 100 nm SiO_2 coated silicon wafer and lithographically patterned and wet chemically etched with a standard Cr wet etch solution (9% $(NH_4)_2Ce(NO_3)_6$ + 6% $(HClO_4)$ + H_2O). The SiO_2 back gate dielectric (100 nm) layer was deposited via plasma enhanced chemical vapor deposition. Subsequently, the a-IGZO active layer (50 nm) was deposited by radio frequency magnetron sputtering (rf magnetron sputtering) using a 5 cm diameter target $(In_2O_3/Ga_2O_3/ZnO$ 1/4 1:1:1 mol %) at room temperature. The initial vacuum level was maintained at a pressure less than 3×10^{-6} Torr, and the rf power and working pressure were maintained at 80 W and 5 mTorr, respectively, during the sputtering process with a 10% oxygen partial pressure in a balance of Argon. The a-IGZO active area was photolithographically patterned using a lift-off process. The Ti/Au (10/70 nm) source and drain (S/D) electrodes and auxiliary electrode to apply bias to the IL were deposited by e-beam evaporation and patterned by a lift-off method. The fabricated devices were annealed at 250 °C for 1 h for a-IGZO channel activation. Finally, the ionic liquid HMImTFSI was dispensed to cover the a-IGZO active area and auxiliary gate electrode to form a side IL-gate dielectric layer for FET measurement. Both the back (SiO2 gate dielectric)- and top (IL-gate dielectric)-gated FET device performances were measured prior to in situ force spectroscopy measurements.

In Situ Force Spectroscopy Measurements. Force−distance curves were measured on a Cypher AFM from Asylum Research (Oxford Instruments, U.K.) in a droplet of HMImTFSI covering the side gate electrode and the a-IGZO channel. A gold-coated silicon tip with a spring constant of ca. 0.6 N/m was used for all experiments with a nominal tip radius of 30 nm. Approaching distance was 30 nm with a scan rate of 0.25 Hz (15 nm/s). To compare all curves and account for drift, the curves were aligned along the y axis to be at zero force far away from the sample. In addition, the curves were shifted along the x axis so that the retract branch of all force−separation curves overlaid. The tip was placed as close to the source electrode as possible, where the electric field can be considered maximal. Gate and drain voltages were controlled by an SP-300 potentiostat (Biologic, France). The drain voltage was fixed at a constant value of 0.1 V while the gate voltage was modulated. The source electrode was used as the counter electrode for both applied voltages, and grounded. The measurements

were performed in an open atmosphere without additional humidity control.

Room Temperature Ionic Liquid. HMImTFSI was prepared through the intermediate HMImBr. Initially, 27.5 mL (0.196 mol) of 1-bromohexane was added into 15.6 mL (0.196 mol) of 1-methylimidazole with 50 mL of acetonitrile solvent drop by drop under argon flowing at room temperature. The reaction was then heated to 60 °C for 15 h and the organic solvent was removed under reduced pressure, affording crude HMImBr. The bromide salt was dissolved in 100 mL of water and then extracted with three 25 mL aliquots of ethyl acetate. The remaining water was subsequently removed by heating under a vacuum, and ion exchange was performed using HMImBr and LiTFSI in water to yield HMImTFSI. Finally, the obtained HMImTFSI was separated and freeze-dried for 3 days before use.

Molecular Dynamics Simulations. Before modeling ILs at the metal oxide surfaces, a-IGZO was obtained from crystalline IGZO by quenched molecular dynamics (QMD). The calculated a-IGZO density is 5.8 g/cm, and the average coordination numbers of the calculated model structure agree well with modeling and experimental work (Table S1).[55,56] The MD system in a channel-like simulation consists of a slab of ILs enclosed between the Au(111) and a-IGZO electrodes with an area of 5.4×4.7 nm^2 parallel to the electrode surface. The gate voltage was applied on the gold and a-IGZO solid electrode surfaces, using the constant potential method.[57] An equal potential was maintained on the electrode surfaces and located at a plane across the center of the surface atoms. This method was able to take into account the electronic polarizability of the electrode surfaces, which has been verified by other work.[58,59] The distance between the gold and a-IGZO surfaces was set to 8.0 nm, which is large enough to prevent overlapping of the EDLs formed at both surfaces. The coordinate system was chosen such that the innermost layer of the a-IGZO wall corresponds to $z = 0$. All-atom force fields were used for HMImTFSI,[60] the force fields for a-IGZO were taken from ref 61 and those for gold from ref 62. Note that the potential applied between the gold and a-IGZO surfaces is the one across the IL slab and does not include the potential drop across a-IGZO. Therefore, the voltages used in the simulations are not comparable to the gate voltage in the experiment. From the plot shown in Figure 3d, we can identify the insulator to metal transition between approximately 0.4 to 1 V with high resistance below and low resistance above this voltage range. When the oxide is in an insulating state below 0.4 V, the voltage drop across the liquid is 0, which is modeled with 0 V. When the oxide is in a metallic state above 1 V, the complete gate voltage is applied to the ionic liquid. Therefore, 1.5 V was used to simulate the ion orientation in the highest conductivity state. To simulate an intermediate state that happens over a gate voltage range of 0.4 to 1.0 V, we chose an MD simulation voltage of 0.4 V applied to the IL slab to be within the transition range. This corresponds to a gate voltage of around 0.7 V (see Supporting Information). Simulations were performed using the customized MD code Gromacs,[63] with a time step of 2 fs. The electrolyte temperature was maintained at 298 K using the Nosé–Hoover thermostat. The number of IL molecules inside the channel was adjusted so that the ILs in the central portion of the channel showed a bulk-like state. The electrostatic interactions were computed using the PME method and by solving an auxiliary Laplace equation.[57] An FFT grid spacing of 0.1 nm and cubic interpolation for charge distribution were used to compute the electrostatic interactions in the reciprocal space; a cutoff length of 1.1 nm was used in the calculation of electrostatic interactions in the real space. The nonelectrostatic interactions were computed by direct summation with a cutoff length of 1.1 nm. Each simulation was run for 30 ns to reach equilibrium, and then a 150 ns production run was performed for analysis.

ASSOCIATED CONTENT

Ⓢ Supporting Information

The Supporting Information is available free of charge on the ACS Publications website at DOI: 10.1021/acsami.7b11044.

Modeling details, details about the generation of quench molecular dynamics simulation, the analysis using density functional theory calculations, information about the correlation between gate voltage and potential across the ionic liquid slab in the simulation, information about the structure of the ionic liquid HMImTFSI at Au(111) surface and additional results on the structure of HMImTFSI at a-IGZO surface (PDF)

AUTHOR INFORMATION

Corresponding Authors
*E-mail: gfeng@hust.edu.cn (G.F.).
*E-mail: balken@ornl.gov (N.B.).

ORCID Ⓘ
Sheng Dai: 0000-0002-8046-3931
Nina Balke: 0000-0001-5865-5892

Present Addresses
▽Nantero Inc., 25-B Olympia Avenue, Woburn, MA 01801, United States (J.M.B.).
○Laboratoire de Réactivité et Chimie des Solides, 33 Rue St Leu, 80039 Amiens Cedex 1, France (J.C.).

Author Contributions
N.B. and S.V.K. contributed to the experimental design and planning and data interpretation. J.M.B. and J.C. developed the AFM measurement protocols and conducted the AFM experiments. P.Z. and S.D. provided the ionic liquids. A.T.W., P.R.P., J.H.N., T.Z.W., and P.D.R. contributed to the device design, synthesis, and characterization. S.B., M.Z., W.Z., and G.F. performed the molecular dynamics simulations. M.B.O. provided analysis programs for force—distance curves. All authors contributed to manuscript writing and discussion.

Notes
The authors declare no competing financial interest.

ACKNOWLEDGMENTS

■ REFERENCES

(1) Zhou, Y.; Ramanathan, S. Mott Memory and Neuromorphic Devices. *Proc. IEEE* **2015**, *103*, 1289−1310.

(2) Pickett, M. D.; Medeiros-Ribeiro, G.; Williams, R. S. A Scalable Neuristor Built with Mott Memristors. *Nat. Mater.* **2013**, *12*, 114−117.

(3) Cao, J.; Ertekin, E.; Srinivasan, V.; Fan, W.; Huang, S.; Zheng, H.; Yim, J. W. L.; Khanal, D. R.; Ogletree, D. F.; Grossmanan, J. C.; Wu, J. Strain Engineering and One-Dimensional Organization of Metal-Insulator Domains in Single-Crystal Vanadium Dioxide Beams. *Nat. Nanotechnol.* **2009**, *4*, 732−737.

(4) Wu, S. M.; Cybart, S. A.; Yu, P.; Rossell, M. D.; Zhang, J. X.; Ramesh, R.; Dynes, R. C. Reversible Electric Control of Exchange Bias in a Multiferroic Field-Effect Device. *Nat. Mater.* **2010**, *9*, 756−761.

(5) Mott, N. F.; Friedman, L. Metal-Insulator Transitions in Vo2, Ti2O3 and Ti2-xVxO3. *Philos. Mag.* **1974**, *30*, 389−402.

(6) Imada, M.; Fujimori, A.; Tokura, Y. Metal-Insulator Transitions. *Rev. Mod. Phys.* **1998**, *70*, 1039−1263.

(7) Rondinelli, J. M.; May, S. J.; Freeland, J. W. Control of Octahedral Connectivity in Perovskite Oxide Heterostructures: An Emerging Route to Multifunctional Materials Discovery. *MRS Bull.* **2012**, *37*, 261−270.

(8) Tokura, Y.; Nagaosa, N. Orbital Physics in Transition-Metal Oxides. *Science* **2000**, *288*, 462−468.

(9) Hwang, H. Y.; Iwasa, Y.; Kawasaki, M.; Keimer, B.; Nagaosa, N.; Tokura, Y. Emergent Phenomena at Oxide Interfaces. *Nat. Mater.* **2012**, *11*, 103−113.

(10) Yuan, H. T.; Shimotani, H.; Tsukazaki, A.; Ohtomo, A.; Kawasaki, M.; Iwasa, Y. High-Density Carrier Accumulation in ZnO Field-Effect Transistors Gated by Electric Double Layers of Ionic Liquids. *Adv. Funct. Mater.* **2009**, *19*, 1046−1053.

(11) Ye, J. T.; Inoue, S.; Kobayashi, K.; Kasahara, Y.; Yuan, H. T.; Shimotani, H.; Iwasa, Y. Liquid-Gated Interface Superconductivity on an Atomically Flat Film. *Nat. Mater.* **2010**, *9*, 125−128.

(12) Ahn, C. H.; Bhattacharya, A.; Di Ventra, M.; Eckstein, J. N.; Frisbie, C. D.; Gershenson, M. E.; Goldman, A. M.; Inoue, I. H.; Mannhart, J.; Millis, A. J.; Morpurgo, A. F.; Natelson, D.; Triscone, J. M. Electrostatic Modification of Novel Materials. *Rev. Mod. Phys.* **2006**, *78*, 1185−1212.

(13) Cho, J. H.; Lee, J.; Xia, Y.; Kim, B.; He, Y. Y.; Renn, M. J.; Lodge, T. P.; Frisbie, C. D. Printable Ion-Gel Gate Dielectrics for Low-Voltage Polymer Thin-Film Transistors on Plastic. *Nat. Mater.* **2008**, *7*, 900−906.

(14) Kim, S. H.; Hong, K.; Xie, W.; Lee, K. H.; Zhang, S. P.; Lodge, T. P.; Frisbie, C. D. Electrolyte-Gated Transistors for Organic and Printed Electronics. *Adv. Mater.* **2013**, *25*, 1822−1846.

(15) Leng, X.; Garcia-Barriocanal, J.; Bose, S.; Lee, Y.; Goldman, A. M. Electrostatic Control of the Evolution from a Superconducting Phase to an Insulating Phase in Ultrathin YBa2CaCu3O7-X Films. *Phys. Rev. Lett.* **2011**, *107*, No. 027001.

(16) Yamada, Y.; Ueno, K.; Fukumura, T.; Yuan, H. T.; Shimotani, H.; Iwasa, Y.; Gu, L.; Tsukimoto, S.; Ikuhara, Y.; Kawasaki, M. Electrically Induced Ferromagnetism at Room Temperature in Cobalt-Doped Titanium Dioxide. *Science* **2011**, *332*, 1065−1067.

(17) Albrecht, T.; Guckian, A.; Ulstrup, J.; Vos, J. G.; Albrecht, T.; Guckian, A.; Ulstrup, J.; Vos, J. G. Transistor Effects and in Situ STM of Redox Molecules at Room Temperature. *IEEE Trans. Nanotechnol.* **2005**, *4*, 430−434.

(18) Albrecht, T.; Guckian, A.; Ulstrup, J.; Vos, J. G. Transistor-Like Behavior of Transition Metal Complexes. *Nano Lett.* **2005**, *5*, 1451−1455.

(19) Albrecht, T.; Moth-Poulsen, K.; Christensen, J. B.; Hjelm, J.; Bjornholm, T.; Ulstrup, J. Scanning Tunneling Spectroscopy in an Ionic Liquid. *J. Am. Chem. Soc.* **2006**, *128*, 6574−6575.

(20) Cheung, K. C. M.; Chen, X. Y.; Albrecht, T.; Kornyshev, A. A. Principles of a Single-Molecule Rectifier in Electrolytic Environment. *J. Phys. Chem. C* **2016**, *120*, 3089−3106.

(21) Zhang, J.; Kuznetsov, A. M.; Medvedev, I. G.; Chi, Q.; Albrecht, T.; Jensen, P. S.; Ulstrup, J. Single-Molecule Electron Transfer in Electrochemical Environments. *Chem. Rev.* **2008**, *108*, 2737−2791.

(22) Pudasaini, P. R.; Noh, J. H.; Wong, A. T.; Ovchinnikova, O. S.; Haglund, A. V.; Dai, S.; Ward, T. Z.; Mandrus, D.; Rack, P. D. Ionic Liquid Activation of Amorphous Metal-Oxide Semiconductors for Flexible Transparent Electronic Devices. *Adv. Funct. Mater.* **2016**, *26*, 2820−2825.

(23) Park, S.; Lee, S.; Kim, C. H.; Lee, I.; Lee, W. J.; Kim, S.; Lee, B. G.; Jang, J. H.; Yoon, M. H. Sub-0.5 V Highly Stable Aqueous Salt Gated Metal Oxide Electronics. *Sci. Rep.* **2015**, *5*, No. 13088.

(24) Yuan, H.; Shimotani, H.; Ye, J.; Yoon, S.; Aliah, H.; Tsukazaki, A.; Kawasaki, M.; Iwasa, Y. Electrostatic and Electrochemical Nature of Liquid-Gated Electric-Double-Layer Transistors Based on Oxide Semiconductors. *J. Am. Chem. Soc.* **2010**, *132*, 18402−18407.

(25) Fujimoto, T.; Awaga, K. Electric-Double-Layer Field-Effect Transistors with Ionic Liquids. *Phys. Chem. Chem. Phys.* **2013**, *15*, 8983−9006.

(26) Noh, J. H.; Joshi, P. C.; Kuruganti, T.; Rack, P. D. Pulse Thermal Processing for Low Thermal Budget Integration of Igzo Thin Film Transistors. *IEEE J. Electron Devices Soc.* **2015**, *3*, 297−301.

(27) Kwon, S.; Noh, J. H.; Noh, J.; Rack, P. D. Quantitative Calculation of Oxygen Incorporation in Sputtered IGZO Films and the Impact on Transistor Properties. *J. Electrochem. Soc.* **2011**, *158*, H289−H293.

(28) Perkin, S.; Albrecht, T.; Klein, J. Layering and Shear Properties of an Ionic Liquid, 1-Ethyl-3-Methylimidazolium Ethylsulfate, Confined to Nano-Films between Mica Surfaces. *Phys. Chem. Chem. Phys.* **2010**, *12*, 1243−1247.

(29) Endres, F.; Borisenko, N.; El Abedin, S. Z.; Hayes, R.; Atkin, R. The Interface Ionic Liquid(S)/Electrode(S): In Situ STM and AFM Measurements. *Faraday Discuss.* **2012**, *154*, 221−233.

(30) Atkin, R.; Borisenko, N.; Druschler, M.; El Abedin, S. Z.; Endres, F.; Hayes, R.; Huber, B.; Roling, B. An in Situ Stm/Afm and Impedance Spectroscopy Study of the Extremely Pure 1-Butyl-1-Methylpyrrolidinium Tris(Pentafluoroethyl) Trifluorophosphate/Au(111) Interface: Potential Dependent Solvation Layers and the Herringbone Reconstruction. *Phys. Chem. Chem. Phys.* **2011**, *13*, 6849−6857.

(31) Zhang, X.; Zhong, Y.-X.; Yan, J.-W.; Su, Y.-Z.; Zhang, M.; Mao, B.-W. Probing Double Layer Structures of Au (111)-BMIPF6 Ionic Liquid Interfaces from Potential-Dependent Afm Force Curves. *Chem. Commun.* **2012**, *48*, 582−584.

(32) Black, J. M.; Okatan, M. B.; Feng, G.; Cummings, P. T.; Kalinin, S. V.; Balke, N. Topological Defects in Electric Double Layers of Ionic Liquids at Carbon Interfaces. *Nano Energy* **2015**, *15*, 737−745.

(33) Mezger, M.; Schroder, H.; Reichert, H.; Schramm, S.; Okasinski, J. S.; Schoder, S.; Honkimaki, V.; Deutsch, M.; Ocko, B. M.; Ralston, J.; Rohwerder, M.; Stratmann, M.; Dosch, H. Molecular Layering of Fluorinated Ionic Liquids at a Charged Sapphire (0001) Surface. *Science* **2008**, *322*, 424−428.

(34) Uysal, A.; Zhou, H.; Feng, G.; Lee, S. S.; Li, S.; Fenter, P.; Cummings, P. T.; Fulvio, P. F.; Dai, S.; McDonough, J. K.; Gogotsi, Y. Structural Origins of Potential Dependent Hysteresis at the Electrified Graphene/Ionic Liquid Interface. *J. Phys. Chem. C* **2014**, *118*, 569−574.

(35) Fedorov, M. V.; Kornyshev, A. A. Ionic Liquids at Electrified Interfaces. *Chem. Rev.* **2014**, *114*, 2978−3036.

(36) Hayes, R.; Warr, G. G.; Atkin, R. Structure and Nanostructure in Ionic Liquids. *Chem. Rev.* **2015**, *115*, 6357−6426.

(37) Elbourne, A.; McDonald, S.; Voichovsky, K.; Endres, F.; Warr, G. G.; Atkin, R. Nanostructure of the Ionic Liquid-Graphite Stern Layer. *ACS Nano* **2015**, *9*, 7608−7620.

(38) Hayes, R.; Borisenko, N.; Tam, M. K.; Howlett, P. C.; Endres, F.; Atkin, R. Double Layer Structure of Ionic Liquids at the Au(111) Electrode Interface: An Atomic Force Microscopy Investigation. *J. Phys. Chem. C* **2011**, *115*, 6855−6863.

(39) Bazant, M. Z.; Storey, B. D.; Kornyshev, A. A. Double Layer in Ionic Liquids: Overscreening Versus Crowding. *Phys. Rev. Lett.* **2011**, *106*, No. 046102.

(40) Lynden-Bell, R. M.; Frolov, A. I.; Fedorov, M. V. Electrode Screening by Ionic Liquids. *Phys. Chem. Chem. Phys.* **2012**, *14*, 2693−2701.

(41) Baldelli, S. Surface Structure at the Ionic Liquid-Electrified Metal Interface. *Acc. Chem. Res.* **2008**, *41*, 421−431.

(42) Black, J. M.; Walters, D.; Labuda, A.; Feng, G.; Hillesheim, P. C.; Dai, S.; Cummings, P. T.; Kalinin, S. V.; Proksch, R.; Balke, N. Bias-Dependent Molecular-Level Structure of Electrical Double Layer in Ionic Liquid on Graphite. *Nano Lett.* **2013**, *13*, 5954−5960.

(43) Uysal, A.; Zhou, H.; Feng, G.; Lee, S. S.; Li, S.; Cummings, P. T.; Fulvio, P. F.; Dai, S.; McDonough, J. K.; Gogotsi, Y.; Fenter, P. Interfacial Ionic 'Liquids': Connecting Static and Dynamic Structures. *J. Phys.: Condens. Matter* **2015**, *27*, No. 032101.

(44) Petach, T. A.; Mehta, A.; Marks, R.; Johnson, B.; Toney, M. F.; Goldhaber-Gordon, D. Voltage-Controlled Interfacial Layering in an Ionic Liquid on SrTiO3. *ACS Nano* **2016**, *10*, 4565−4569.

(45) Fillion, J. J.; Xia, H.; Desilva, M. A.; Quiroz-Guzman, M.; Brennecke, J. F. Phase Transitions, Decomposition Temperatures, Viscosities, and Densities of Phosphonium, Ammonium, and Imidazolium Ionic Liquids with Aprotic Heterocyclic Anions. *J. Chem. Eng. Data* **2016**, *61*, 2897−2914.

(46) Perkin, S.; Crowhurst, L.; Niedermeyer, H.; Welton, T.; Smith, A. M.; Gosvami, N. N. Self-Assembly in the Electrical Double Layer of Ionic Liquids. *Chem. Commun.* **2011**, *47*, 6572−6574.

(47) Black, J. M.; Zhu, M. Y.; Zhang, P. F.; Unocic, R. R.; Guo, D. Q.; Okatan, M. B.; Dai, S.; Cummings, P. T.; Kalinin, S. V.; Feng, G.; Balke, N. Fundamental Aspects of Electric Double Layer Force-Distance Measurements at Liquid-Solid Interfaces Using Atomic Force Microscopy. *Sci. Rep.* **2016**, *6*, No. 32389.

(48) Hammer, T.; Reichelt, M.; Morgner, H. Influence of the Aliphatic Chain Length of Imidazolium Based Ionic Liquids on the Surface Structure. *Phys. Chem. Chem. Phys.* **2010**, *12*, 11070−11080.

(49) Atkin, R.; Borisenko, N.; Druschler, M.; Endres, F.; Hayes, R.; Huber, B.; Roling, B. Structure and Dynamics of the Interfacial Layer between Ionic Liquids and Electrode Materials. *J. Mol. Liq.* **2014**, *192*, 44−54.

(50) Fedorov, M. V.; Georgi, N.; Kornyshev, A. A. Double Layer in Ionic Liquids: The Nature of the Camel Shape of Capacitance. *Electrochem. Commun.* **2010**, *12*, 296−299.

(51) Pudasaini, P. R.; Noh, J. H.; Wong, A.; Haglund, A. V.; Dai, S.; Ward, T. Z.; Mandrus, D.; Rack, P. D. Ionic Liquid Versus Sio2 Gated a-Igzo Thin Film Transistors: A Direct Comparison. *ECS J. Solid State Sci. Technol.* **2015**, *4*, Q105−Q109.

(52) Li, M.; Graf, T.; Schladt, T. D.; Jiang, X.; Parkin, S. S. P. Role of Percolation in the Conductance of Electrolyte-Gated SrTiO3. *Phys. Rev. Lett.* **2012**, *109*, No. 196803.

(53) Sparnaay, M. J. *The Electrical Double Layer*; Pergamon Press: Oxford, 1972; Vol. *4*.

(54) Limmer, D. T.; Merlet, C.; Salanne, M.; Chandler, D.; Madden, P. A.; van Roij, R.; Rotenberg, B. Charge Fluctuations in Nanoscale Capacitors. *Phys. Rev. Lett.* **2013**, *111*, No. 106102.

(55) Nomura, K.; Kamiya, T.; Ohta, H.; Uruga, T.; Hirano, M.; Hosono, H. Local Coordination Structure and Electronic Structure of the Large Electron Mobility Amorphous Oxide Semiconductor in-Ga-Zn-O: Experiment and Ab Initio Calculations. *Phys. Rev. B* **2007**, *75*, No. 035212.

(56) Korner, W.; Urban, D. F.; Elsasser, C. Origin of Subgap States in Amorphous in-Ga-Zn-O. *J. Appl. Phys.* **2013**, *114*, No. 163704.

(57) Raghunathan, A. V.; Aluru, N. R. Self-Consistent Molecular Dynamics Formulation for Electric-Field-Mediated Electrolyte Transport through Nanochannels. *Phys. Rev. E* **2007**, *76*, No. 011202.

(58) Wu, P.; Huang, J. S.; Meunier, V.; Sumpter, B. G.; Qiao, R. Complex Capacitance Scaling in Ionic Liquids-Filled Nanopores. *ACS Nano* **2011**, *5*, 9044−9051.

(59) Kondrat, S.; Wu, P.; Qiao, R.; Kornyshev, A. A. Accelerating Charging Dynamics in Subnanometre Pores. *Nat. Mater.* **2014**, *13*, 387−393.

(60) Lopes, J. N. C.; Padua, A. A. H. Molecular Force Field for Ionic Liquids Composed of Triflate or Bistriflylimide Anions. *J. Phys. Chem. B* **2004**, *108*, 16893−16898.

(61) Rappe, A. K.; Casewit, C. J.; Colwell, K. S.; Goddard, W. A.; Skiff, W. M. Uff, a Full Periodic Table Force Field for Molecular Mechanics and Molecular Dynamics Simulations. *J. Am. Chem. Soc.* **1992**, *114*, 10024−10035.

(62) Verde, A. V.; Acres, J. M.; Maranas, J. K. Investigating the Specificity of Peptide Adsorption on Gold Using Molecular Dynamics Simulations. *Biomacromolecules* **2009**, *10*, 2118−2128.

(63) Lindahl, E.; Hess, B.; van der Spoel, D. Gromacs 3.0: A Package for Molecular Simulation and Trajectory Analysis. *J. Mol. Model.* **2001**, *7*, 306−317.